International Journal of Non-Linear Mechanics 124 (2020) 103502

Contents lists available at ScienceDirect

International Journal of Non-Linear Mechanics

journal homepage: www.elsevier.com/locate/nlm

Observation of vector solitary waves in soft laminates using a finite-volume method

Ron Ziv, Gal Shmuel *

Faculty of Mechanical Engineering, Technion-Israel Institute of Technology, Haifa 32000, Israel

ARTICLE INFO

Keywords:
Finite-volume method
Composites
Laminates
Soft materials
Nonlinear elasticity
Finite deformations
Wave propagation
Solitary waves
Shocks
Gent material

ABSTRACT

Soft materials with engineered microstructure support nonlinear waves which can be harnessed for various applications, from signal communication to impact mitigation. Such waves are governed by nonlinear coupled differential equations whose analytical solution is seldom trackable, hence emerges the need for suitable numerical solvers. Based on a finite-volume method in one space dimension, we here develop a designated scheme for nonlinear waves with two coupled components that propagate in soft laminates. We apply our scheme to a periodic laminate made of two alternating compressible Gent layers, and consider two cases. In one case, we analyze a motion whose component along the lamination direction is coupled to a component in the layers plane, and discover vector solitary waves in a continuum medium. In the second case, we analyze a motion with two coupled components in the plane of the layers, and observe a train of linearly polarized solitary waves, followed by a single circularly polarized wave. The framework we developed offers a platform for further investigation of these waves and their extension to higher dimensional problems.

1. Introduction

Highly deformable materials with architectured microstructure are nowadays accessible by virtue of the current manufacturing abilities [1, 2]. These materials exhibit geometrical and constitutive nonlinearities that give rise to rich physics [3], and in particular diverse wave phenomena such as unidirectional transmission, shocks and self-reinforcing waves [4–9]. Waves in nonlinear solids have recently regained scientific and technological interest, owing to the realization that their features can be harnessed for various applications, such as signal transmission [10], impact mitigation [11], energy harvesting [12] and mechanical diodes [13].

The mathematical modeling of waves in nonlinear solids with microstructure is given by nonlinear coupled partial differential equations, whose analytical solution is seldom trackable [14–17], hence the need for designated numerical solvers. Notably, these solvers should account for the fact that when the deformations are large there is a distinction between the reference and current configuration space, where the finite-strain Lagrangian formulation [18–20] allows for this distinction. Among the different schemes developed for nonlinear Lagrangian elastodynamics, we recall those based on the finite difference method [21], finite element method [22], and specifically the finite-volume method [23].

Finite-volume methods are useful in solving problems whose physics is governed by space–time conservation laws [24–26], and as such are useful in elastodynamics [27]. Importantly, these methods are conservative in a way that emulates the exact solution—a useful feature in problems whose solution is discontinuous [27,28]. Based on the solution of a Riemann problem at the interface between grid cells, LeVeque [29] developed a general high-resolution scheme for nonlinear hyperbolic systems which depend on multiple space dimensions and are not in conservation form. Such a deviation from the conservation form can occur when the medium is heterogeneous—the type of medium we focus on in this work, giving rise to a spatially-varying flux. The application of finite-volume algorithms based on solutions of Riemann problems has been extended to thermoelastic materials [30], elastoplastic materials [31], and materials that exhibit softening [23], among other media.

Fogarty and LeVeque [32] have demonstrated the efficiency of Leveque's approach in different problems of *acoustic* waves and one- and two-dimensional heterogeneous linear media. The term acoustic denotes waves in media that cannot sustain shear, hence corresponds to pressure (compression) waves alone. In the periodic case, they have also refined the method using a new *limiter function*—a scalar function aimed at limiting the gradient of the solution near discontinuities—relatively to the one used by LeVeque [29]. Later on, LeVeque [33] and Bale et al. [34] have adapted the approach to pressure waves in one- and two-dimensional nonlinear heterogeneous media, by decomposing the flux difference at the interface between grid cells. This is in contrast with the standard approach that decomposes the conserved vector. These works revealed solitary waves, namely, nonlinear waves that are able to maintain constant speed and profile by

* Corresponding author.
E-mail address: meshmuel@technion.ac.il (G. Shmuel).

https://doi.org/10.1016/j.ijnonlinmec.2020.103502
Received 19 December 2019; Received in revised form 24 April 2020; Accepted 5 May 2020
Available online 15 May 2020

virtue of a balance between nonlinear and dispersive features of the system [35,36]. These one-dimensional elastic solitary waves were later studied in greater detail by LeVeque and Yong [37,38]; see also the works of Engelbrecht et al. [39] and Xu et al. [40].

Here, we extend the flux-based wave decomposition scheme of LeVeque [33] and Bale et al. [34] to nonlinear elastic heterogeneous media exhibiting coupled finite-amplitude waves. In contrast with acoustics where there is only volumetric waves and the only stress component is in the propagation direction, in elastodynamics there are also shear waves which may couple with volumetric waves, and yield traction components in the plane transverse to the propagation direction [41]. The media of interest are composites made of soft layers, where the component of the deformation in the lamination direction (referred to as the axial component) is coupled with a transverse component in the plane of the layers [14]. We also consider a second case in which two components in the layers plane are coupled one with the other [42], *i.e.*, the coupling of two shear waves. By developing of a suitable matrix representation, our extension accounts for the generation of such additional waves and their coupling. To the best of our knowledge, while finite-volume schemes have been developed for two-dimensional nonlinear elastodynamics, *e.g.*, by Berjamin et al. [43], the case of spatially-varying flux in that setting has yet to be explicitly addressed.[1]

We validate our method using two test cases. In the first test, we consider one layer bounded between two semi-infinite layers with different parameters, and note that these layers respond nonlinearly to finite-amplitude deformations. We subject the middle layer to an initial small-amplitude shear strain and show that the numerical solution captures the response as predicted by the analytical solution of the limiting linear problem [44]. The second test is of nonlinear waves and hence more challenging, where we address the canonical problem of wave scattering at an interface between two nonlinearly elastic half-spaces; here, however, the waves are of finite-amplitude and the displacements are coupled. The aspect of shock evolution in this setting was addressed by Davison [45], who studied axial waves. Here, we extend the settings to shocks associated with waves comprising two coupled components, noting that to the best of our knowledge this is the first numerical experiment of such problems. An analytical solution to this problem is not available, and hence our finite-volume based solution to the linearized algebraic equations is compared with numerical solutions using Newton's method to the exact nonlinear equations, to find an excellent agreement. The model we use to describe the nonlinear response of the media in our test cases is the compressible Gent model [46]. This model—originally developed for capturing the strain stiffening of rubber at large strains—was recently shown useful by Ziv and Shmuel [7] for modeling shear shocks that were experimentally observed by Catheline et al. [47] and Espíndola et al. [48],[2] and modeling tensile-induced shocks that were experimentally observed by Niemczura and Ravi-Chandar [49].

Subsequently, we apply our scheme to a pre-strained laminate made of two alternating compressible Gent layers. Remarkably, in the case where the axial and transverse components of the motion are coupled, our numerical solution reveals a generation of elastic *vector* solitary waves. As mentioned, solitary waves are nonlinear waves that propagate with constant speed and profile by virtue of a balance between nonlinearity and dispersion in the system. The term *vector* refers to the case where these solitary waves consist of two (or more) components *and* polarizations that are coupled one with the other [50,51]. To the best of our knowledge, our results are the first report of vector solitary waves in an elastic *continuum*, based on the equations of nonlinear elastodynamics. Our observation is preceded by the first construction of vector solitary waves in *discrete* mechanical systems that were conceived by Deng et al. [52,53]. There, the model is a periodic repetition of rigid squares that are interlinked by springs, thereby supporting transitional and rotational waves. Interestingly, while these mechanical waves are slower at higher amplitudes, the vector solitary waves in our continuum laminated medium are faster at higher amplitudes, similarly to the KdV solitons and the solitary waves analyzed by LeVeque and Yong [38], as we show in what follows.

In the second case where the coupling is between two transverse components, we discover the propagation of (scalar) solitary waves that are linearly polarized, namely, their polarization direction is fixed. We also observe the propagation of a single slower wave which is circularly polarized, namely, its direction rotates in the transverse plane.

Our results are presented in the following order. Section 2 summarizes the equations governing motions with two coupled components in laminates made of compressible Gent layers, together with the derivation of the Gent phase velocities in each case. Section 3 details our finite-volume method for the solution of these equations. The validation of our method using the two test cases is provided in Section 4, and the numerical experiments of coupled motions in periodic Gent layers is carried out in Section 5. We summarize our main results and conclusions in Section 6, together with an outlook towards future work.

2. Governing equations

We use the standard governing equations in Lagrangian continuum mechanics to formulate the problem of interest, see, *e.g.*, the books of Ogden [54] and Bonet and Wood [55]. We consider a soft composite made of two perfectly bonded alternating hyperelastic phases that are laminated in the X_1 direction. The layers are infinite in the X_2 and X_3 directions; the loads in these directions are assumed to be uniform, and hence the response of the laminate is only a function of X_1. We denote the initial thickness, mass density and strain energy density function of layer n by $H^{(n)}$, $\rho_L^{(n)}$ and $\Psi^{(n)}$. In the numerical simulations to follow, we will use the compressible[3] Gent energy function [46,56] to model the phases, given by

$$\Psi^{(n)}(\mathbf{F}) = -\frac{\mu^{(n)} J_m^{(n)}}{2} \ln\left(1 - \frac{\mathrm{tr}\mathbf{F}^{\mathrm{T}}\mathbf{F} - 3}{J_m^{(n)}}\right) - \mu^{(n)} \ln \det\mathbf{F} + \left(\frac{\kappa^{(n)}}{2} - \frac{\mu^{(n)}}{3} - \frac{\mu^{(n)}}{J_m^{(n)}}\right)(\det\mathbf{F} - 1)^2, \tag{1}$$

where $\mathbf{F}$ is the deformation gradient (to be defined formally later), $\mu^{(n)}$ and $\kappa^{(n)}$ correspond to the shear and bulk moduli in the limit of small strains, respectively, and $J_m^{(n)}$ models the strain stiffening that rubber exhibits due to the limited extensibility of its polymer chains. In the limit $J_m \to \infty$, the Gent model reduces to the fundamental neo-Hookean model [57]. The motion of the composite is described in terms of χ: a continuous and twice differentiable function (except at material interfaces), which maps material points from their initial position $\mathbf{X}$ to their current position $\mathbf{x}$ at time t, such that $\mathbf{x} = \chi(\mathbf{X}, t)$. As mentioned, we focus on deformations that are only functions of X_1, namely,

$$x_1 = X_1 + u_1(X_1, t), \; x_2 = X_2 + u_2(X_1, t), \; x_3 = X_3 + u_3(X_1, t), \tag{2}$$

where u_i are the components of the displacement field. The problem thus amounts to determining $u_i(X_1, t)$ for a given set of boundary and initial conditions. This requires satisfying balance laws for the corresponding first Piola–Kirchhoff stress tensor $\mathbf{P} = \nabla_{\mathbf{F}}\Psi$, where $\mathbf{F} =$

[1] While the setting of Berjamin et al. [43] is two-dimensional nonlinear elastodynamics, the numerical method they provide when the coefficients are spatially-varying is for the one-dimensional case (Appendix B therein).

[2] We clarify that it is the stiffening of these media—not their nearly-incompressible nature—that leads to the formation of shocks. Therefore, the both compressible [7] and incompressible [17] Gent models are capable of capturing shear shocks.

[3] For completeness, we note that in the incompressible limit ($\det\mathbf{F} \equiv 1$), the kinematic constraint is handled using the addition of a Lagrange multiplier [54,55].

$\nabla_{\mathbf{X}}\chi$ is the deformation gradient. For the compressible Gent model, the $\mathbf{F}$-gradient yields

$$\mathbf{P} = \mu\left(1 - \frac{\mathrm{tr}\mathbf{F}^{\mathrm{T}}\mathbf{F} - 3}{J_m}\right)^{-1}\mathbf{F} + \left(\kappa - \frac{2\mu}{J_m} - \frac{2\mu}{3}\right)\det\mathbf{F}\left(\det\mathbf{F} - 1\right)\mathbf{F}^{-\mathrm{T}} - \mu\mathbf{F}^{-\mathrm{T}}. \tag{3}$$

It is worth highlighting now what are the nonlinearities in the Cauchy stress $\sigma = (\det\mathbf{F})^{-1}\,\mathbf{P}\mathbf{F}^{\mathrm{T}}$ that emerge when employing the Gent model. First, it has a term proportional to $\mathbf{F}\mathbf{F}^{\mathrm{T}}$, hence does not neglect quadratic terms in the components of the displacement gradient, in contrast with linear elasticity. Secondly, the coefficient[4] that multiplies $\mathbf{F}\mathbf{F}^{\mathrm{T}}$ is also a nonlinear function of the deformation, in contrast with the Hookean and neo-Hookean models, where this coefficient is constant. These nonlinearities play a crucial role in evolution of nonlinear waves. Smooth nonlinear waves are solutions to the Lagrangian equations of motion

$$\nabla_{\mathbf{X}}\cdot\mathbf{P} = \rho_L\chi_{,tt}, \tag{4}$$

as discussed later. For the mapping of interest (2), Eq. (4) reduces to

$$P_{i1,1} = \rho_L\frac{\partial^2 u_i}{\partial t^2},\ i = 1,2,3. \tag{5}$$

Focusing on motions in which either $u_1 \equiv 0$ or $u_3 \equiv 0$, we rewrite Eq. (5) as

$$u_1 \equiv 0:\ \ P_{21,1} = \rho_L\frac{\partial^2 u_2}{\partial t^2}\ ,\ P_{31,1} = \rho_L\frac{\partial^2 u_3}{\partial t^2}; \tag{6a,b}$$

$$u_3 \equiv 0:\ \ P_{11,1} = \rho_L\frac{\partial^2 u_1}{\partial t^2}\ ,\ P_{21,1} = \rho_L\frac{\partial^2 u_2}{\partial t^2}. \tag{6c,d}$$

Physically, $u_1 \equiv 0$ corresponds to a transverse motion in the plane perpendicular to X_1 (Fig. 1b), whereas $u_3 \equiv 0$ corresponds to coupled axial and transverse motions (Fig. 1c). We can analyze the two cases together using a unifying equation by replacing the first index of $\mathbf{P}$ in Eqs. (6)a and (6)c by a and in Eqs. (6)b and (6)d by b, and writing

$$P_{a1,1} = \rho_L\frac{\partial^2 u_a}{\partial t^2},\ P_{b1,1} = \rho_L\frac{\partial^2 u_b}{\partial t^2}, \tag{7}$$

where we recall that ρ_L is a piecewise-constant function that varies between phases, while u_i and P_{i1} are continuous functions.[5] We denote the spatial and temporal derivatives of u_i by

$$\epsilon_i := \frac{\partial u_i}{\partial X_1},\ v_i := \frac{\partial u_i}{\partial t},\ i = a,b, \tag{8}$$

and put Eq. (7) in the form

$$\begin{pmatrix}\epsilon_a\\ \epsilon_b\\ \rho_L v_a\\ \rho_L v_b\end{pmatrix}_{,t} + \begin{pmatrix}-v_a\\ -v_b\\ -P_{a1}\\ -P_{b1}\end{pmatrix}_{,X_1} = \begin{pmatrix}0\\0\\0\\0\end{pmatrix}, \tag{9}$$

By applying the chain rule, we obtain

$$\begin{pmatrix}\epsilon_a\\ \epsilon_b\\ \rho_L v_a\\ \rho_L v_b\end{pmatrix}_{,t} + \begin{pmatrix}0 & 0 & -\frac{1}{\rho_L} & 0\\ 0 & 0 & 0 & -\frac{1}{\rho_L}\\ -\alpha & -\beta & 0 & 0\\ -\gamma & -\delta & 0 & 0\end{pmatrix}\begin{pmatrix}\epsilon_a\\ \epsilon_b\\ \rho_L v_a\\ \rho_L v_b\end{pmatrix}_{,X_1} = \begin{pmatrix}0\\0\\0\\0\end{pmatrix}, \tag{10}$$

where

$$\alpha = \frac{\partial P_{a1}}{\partial\epsilon_a},\ \beta = \frac{\partial P_{a1}}{\partial\epsilon_b},\ \gamma = \frac{\partial P_{b1}}{\partial\epsilon_a},\ \delta = \frac{\partial P_{b1}}{\partial\epsilon_b}, \tag{11}$$

and for later use, we denote the matrix in Eq. (10) by G. When specialized to the compressible Gent model and the case $u_1 \equiv 0$, the Piola components required for calculating Eq. (11) are

$$P_{21} = \mu\epsilon_2\left(1 - \frac{\epsilon_2^2 + \epsilon_3^2}{J_m}\right)^{-1},\qquad P_{31} = \mu\epsilon_3\left(1 - \frac{\epsilon_2^2 + \epsilon_3^2}{J_m}\right)^{-1}, \tag{12}$$

where when $u_3 \equiv 0$ the components are

$$P_{11} = \mu\left(\epsilon_1 + 1\right)\left(1 - \frac{\epsilon_1^2 + \epsilon_2^2 + 2\epsilon_1}{J_m}\right)^{-1} + \left(\kappa - \frac{2\mu}{J_m} - \frac{2\mu}{3}\right)\epsilon_1 - \frac{\mu}{\epsilon_1 + 1},\qquad P_{21} = \mu\epsilon_2\left(1 - \frac{\epsilon_1^2 + \epsilon_2^2 + 2\epsilon_1}{J_m}\right)^{-1}. \tag{13}$$

The eigenvalues of Eq. (10) are the following characteristic wave velocities in the material

$$c = \pm\sqrt{\frac{1}{2\rho_L}\left[\alpha + \delta \pm \sqrt{(\alpha - \delta)^2 + 4\beta\gamma}\right]} =: \pm c_{\pm}, \tag{14}$$

where c_+ and c_- correspond to the plus and minus sign of the inner square root, respectively. Eq. (10) is hyperbolic when $c_{\pm}$ are real, *i.e.*, when the conditions

$$\alpha + \delta - \sqrt{(\alpha - \delta)^2 + 4\beta\gamma} > 0,\ (\alpha - \delta)^2 + 4\beta\gamma > 0, \tag{15}$$

are satisfied [14]. The compressible Gent model satisfies conditions (15) for all its admissible strains before the "lock-up" $\left(\mathrm{tr}\mathbf{F}^{\mathrm{T}}\mathbf{F} - 3 < J_m\right)$, hence Eq. (10) is suitable for numerical solutions based on finite-volume methods [27].

In the case of coupled axial and transverse displacements, the explicit expressions for the velocities of the compressible Gent model are

$$c_{\pm}^2 = \frac{d_3}{2\rho_L} + \frac{\mu}{2\rho_L d_1^2} + \frac{\left(d_1^2 + \epsilon_2^2 + J_m\right)\mu J_m}{2\rho_L d_2^2} \pm \frac{\sqrt{48 d_1^6\mu^2\epsilon_2^2 J_m^2 + \left(d_1^2 d_2^2 d_3 + 2d_1^4\mu J_m - 2d_1^2\epsilon_2^2\mu J_m + d_2^2\mu\right)^2}}{2\sqrt{3}\rho_L d_2^2 d_1^2}, \tag{16}$$

where

$$d_1 = \epsilon_1 + 1,\ d_2 = \epsilon_1^2 + 2\epsilon_1 + \epsilon_2^2 - J_m,\ d_3 = \kappa - \frac{2\mu}{3} - \frac{2\mu}{J_m}. \tag{17}$$

In this case, the slower velocity c_- is a monotonically increasing function of the strains, and the corresponding wave is referred to as genuinely nonlinear. The faster velocity c_+ has local minima at certain strains [7], and hence the corresponding wave is not genuinely nonlinear. In the following sections we focus on strains far from these local minima, such that this mode can be considered genuinely nonlinear. The fact that the velocities are nonlinear functions of the strain components allows the formation of shocks under certain conditions; this formation is the focus of previous works [7,17] and the relevant conditions are briefly discussed in the Appendix. In the limit of linear elasticity, c_- and c_+ associated with Eq. (6c,d) correspond to the velocities of shear and pressure waves, respectively.

Collins [42] showed that coupled transverse deformations with finite amplitude associated with Eq. (6a,b) propagate in isotropic media as a combination of circularly polarized waves with the velocity c_- and linearly polarized waves with the velocity c_+. This nature of motion is revealed using the transformation

$$\epsilon_2 = \epsilon_T\cos\theta,\ \epsilon_3 = \epsilon_T\sin\theta, \tag{18}$$

which decouples the waves such that ϵ_T and θ are constants across waves propagating with the velocities c_- and c_+, respectively. In other

[4] Note that the coefficient that multiplies the hydrostatic part is also a nonlinear function of the deformation.

[5] The continuity of P_{i1} results from the standard application of the balance of linear momentum in its integral form at the reference configuration near material interfaces, and u_i are continuous there since the layer are perfectly bonded.

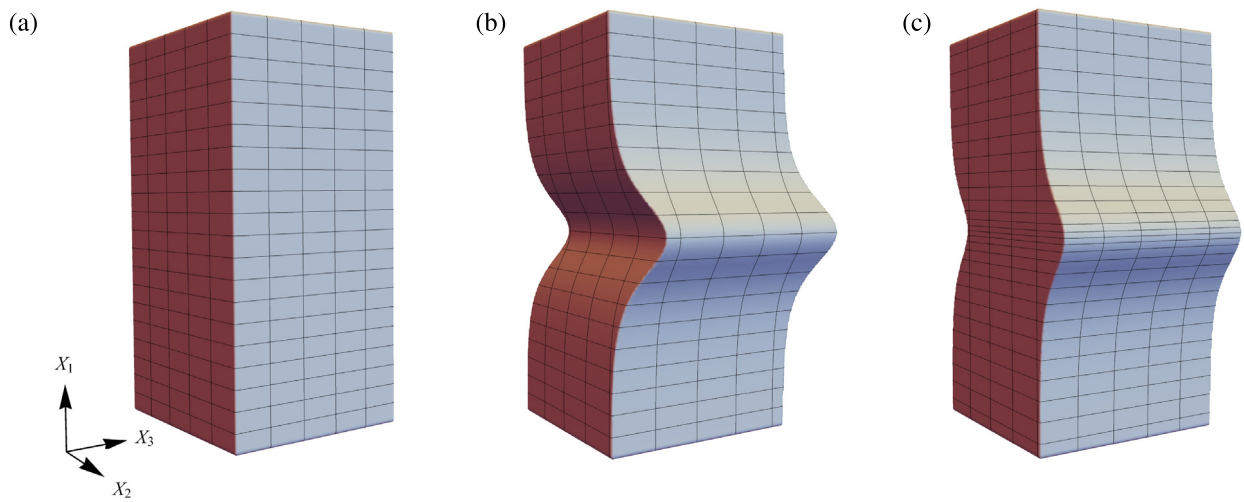

Fig. 1. (a) Reference configuration of a representative phase. (b) Illustrative deformation when $u_1 \equiv 0$, and (c) $u_3 \equiv 0$.

words, the circularly polarized wave is characterized by a fixed strain and rotating polarization, where for the linearly polarized wave the polarization is fixed and the strain magnitude varies. The corresponding velocities in a compressible Gent material are

$$c_- = \sqrt{\frac{\mu J_m}{\rho_L \left(J_m - \epsilon_T^2\right)}}, \quad c_+ = \sqrt{\frac{\mu J_m \left(J_m + \epsilon_T^2\right)}{\rho_L \left(J_m - \epsilon_T^2\right)^2}}, \tag{19}$$

respectively. Note that c_- is constant since ϵ_T is a constant too. Hence, circularly polarized waves are effectively propagating as linear waves, and are referred to as linearly degenerate [27]. By contrast, the quantity ϵ_T varies for linearly polarized waves, hence their velocity c_+ is a nonlinear function of the strain measure. Specifically, it is a monotonically increasing function of ϵ_T, and therefore the linearly polarized mode is genuinely nonlinear.

In the subsequent sections we formulate a finite-volume method for layered materials governed by Eq. (10), validate it using two benchmark problems, and apply it in a numerical experiment of coupled waves in nonlinear laminates.

3. The finite-volume method

First, we define the conserved vector q and its flux vector f according to

$$\mathsf{q} := \begin{pmatrix} \epsilon_a \\ \epsilon_b \\ \rho_L v_a \\ \rho_L v_b \end{pmatrix}, \quad \mathsf{f} := -\begin{pmatrix} v_a \\ v_b \\ P_{a1} \\ P_{b1} \end{pmatrix}, \tag{20}$$

such that the two forms of the governing equations given in Eqs. (9)–(10) are written respectively as

$$\mathsf{q}_{,t} + \mathsf{f}_{,X_1} = 0, \tag{21a}$$

$$\mathsf{q}_{,t} + \nabla_{\mathsf{q}} \mathsf{f} \cdot \mathsf{q}_{,X_1} = 0, \tag{21b}$$

where $\nabla_{\mathsf{q}} \mathsf{f} \equiv \mathsf{G}$. Eq. (21b) is in the form of a conservation law for q.

We consider a grid of uniform length ΔX, and approximate the values of q and f as constants within each length element using the value at the center of the element; the ith element is denoted using superscript i, see Fig. 2(a). Following LeVeque [29], we formulate a finite-volume scheme based on an approximate solution to the Riemann problem between two adjacent cells i and $i+1$. We adopt the flux-decomposition approach of LeVeque [33] and Bale et al. [34], *i.e.,* we solve the system

$$\mathsf{f}^{(i+1)} - \mathsf{f}^{(i)} = \sum_{k=1}^{2} [\![A_k]\!]^i \mathsf{r}_k^{(i)} + \sum_{k=3}^{4} [\![A_k]\!]^i \mathsf{r}_k^{(i+1)}; \tag{22}$$

here, $\{\mathsf{r}_k\}$ are eigenvectors of G, namely,

$$\mathsf{r}_1 = \begin{pmatrix} 1 \\ \eta \\ \rho_L c_+ \\ \eta \rho_L c_+ \end{pmatrix}, \quad \mathsf{r}_2 = \begin{pmatrix} -\zeta \\ 1 \\ -\zeta \rho_L c_- \\ \rho_L c_- \end{pmatrix}, \quad \mathsf{r}_3 = \begin{pmatrix} -\zeta \\ 1 \\ \zeta \rho_L c_- \\ -\rho_L c_- \end{pmatrix}, \quad \mathsf{r}_4 = \begin{pmatrix} 1 \\ \eta \\ -\rho_L c_+ \\ -\eta \rho_L c_+ \end{pmatrix}, \tag{23}$$

where $\eta = -\left(\alpha - \rho_L c_+\right)/\beta$, $\zeta = \beta/\left(\alpha - \rho_L c_-\right)$, and $[\![A_k]\!]^i$ denotes the jump in f in the direction of its kth eigenvector between cells i and $i+1$. Thus, Eq. (22) constitutes a linear algebraic system of equations for $[\![A_k]\!]^i$. Physically, this solution corresponds to four waves propagating with the velocities $c_n = -c_+, -c_-, c_-$ and c_+, which contains jumps in f and q that are proportional to the respective eigenvectors. Characteristic curves as representative solutions to the Riemann problem of two adjacent phases in cells i and $i+1$ are shown in Fig. 2(b), as given by Eq. (22). These solutions are composed of four linear waves with a discontinuity in the state and flux fields, where the slopes of the characteristic lines are their velocity. These waves are separated into two rightward- and two leftward propagating waves.

As noted in the introduction, the common approach is to decompose the difference $\mathsf{q}^{(i+1)} - \mathsf{q}^{(i)}$ instead of $\mathsf{f}^{(i+1)} - \mathsf{f}^{(i)}$. In our problem the mismatch in the material parameters between the adjacent cells results in q containing an additional jump at the interface which is not in the direction of any one of the eigenvectors. As advocated by LeVeque [33] and Bale et al. [34] in the context of pressure (compression) waves in nonlinear heterogeneous solids, the decomposition of the difference in f delivers a simpler set of equations, since f must be continuous across the interface.

Next, we integrate the approximate solution in a finite-volume scheme, as done by LeVeque [29]. We use a *Godunov-type* method with a second order correction [58]

$$\mathsf{q}^{(i)}(t + \Delta t) = \mathsf{q}^{(i)}(t) - \frac{\Delta t}{\Delta X}\left(\mathsf{f}^{(i,i+1)} - \mathsf{f}^{(i-1,i)}\right) - \frac{\Delta t}{2\Delta X}\left(\hat{\mathsf{f}}^{(i,i+1)} - \hat{\mathsf{f}}^{(i-1,i)}\right), \tag{24}$$

where

$$\mathsf{f}^{(i,i+1)} := \mathsf{f}^{(i)} + [\![A_1]\!]^i \mathsf{r}_1^{(i)} + [\![A_2]\!]^i \mathsf{r}_2^{(i)} \equiv \mathsf{f}^{(i+1)} - [\![A_4]\!]^i \mathsf{r}_4^{(i+1)} - [\![A_3]\!]^i \mathsf{r}_3^{(i+1)} \tag{25}$$

is the value of f at the interface (see Fig. 2(b)), and

$$\hat{\mathsf{f}}^{(i,i+1)} = \sum_{k=1}^{4} \operatorname{sign} c_k^{(i+j)} \left(1 - \frac{\Delta t}{\Delta X}\left|c_k^{(i+j)}\right|\right) [\![A_k]\!]^i \mathsf{r}_k^{(i+j)} \tag{26}$$

is the second order correction, with j equals 0 (resp. 1) for $k = 1, 2$ (resp. $k = 3, 4$).

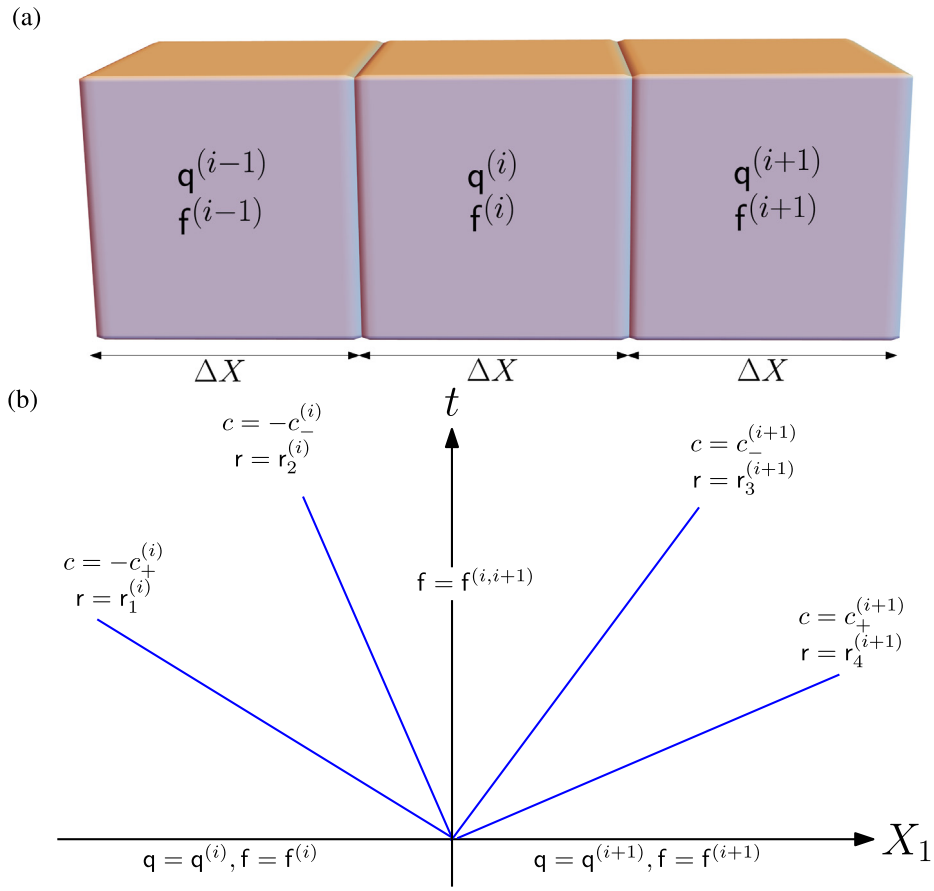

Fig. 2. (a) Illustration of the discretization of the material in the numerical scheme. (b) Representative characteristic curves associated with the solution to the Riemann problem of two adjacent phases between cells i and $i+1$.

Table 1
Sets of Gent moduli used in the numerical simulations, chosen from the characteristic range of the values that fits elastomers.

Set	ρ [kg/m^3]	μ [kPa]	κ [MPa]	J_m
1	1000	100	0.5	10
2	1000	400	2	10
3	500	200	1	10
4	4000	200	1	10

While the second order correction improves the numerical solution when the exact solution is smooth, in case of discontinuities it may lead to unwanted numerical oscillations. To resolve this issue, we employ the approach that was introduced by LeVeque [29] which uses a *wave limiter*, namely, we replace $[\![A_k]\!]^i$ in Eq. (26) by $\phi\left(\theta_k^{(i,i+1)}\right)[\![A_k]\!]^i$, where ϕ is a function of

$$\theta_k^{(i,i+1)} = \frac{c_k^{(i+j)}[\![A_k]\!]^{i-2j+1}}{c_k^{(i-j+1)}[\![A_k]\!]^i}\frac{\mathsf{r}_k^{\mathsf{T}(i+j)}\cdot\mathsf{r}_k^{(i-j+1)}}{\mathsf{r}_k^{\mathsf{T}(i+j)}\cdot\mathsf{r}_k^{(i+j)}}. \tag{27}$$

(See a discussion on earlier versions of wave limiters by LeVeque [29], and the references therein.) The *monotonized centered* function is a simple example of ϕ, defined by

$$\phi\left(\theta_k^{(i,i+1)}\right) = \max\left\{0, \min\left(\frac{1}{2}+\frac{\theta_k^{(i,i+1)}}{2},\ 2,\ 2\theta_k^{(i,i+1)}\right)\right\}. \tag{28}$$

Lastly, in order for the method to be numerically stable, it is necessary for the *Courant–Friedrichs–Lewy* (CFL) *condition* to be satisfied, that is

$$\frac{\Delta t}{\Delta X}\max_i c_+^{(i)} < 1. \tag{29}$$

The left-hand side in Eq. (29) is referred to as the Courant number [59]. The *domain of dependence* of a point $\{x_0, t_0\}$ is the set of points $\{x, t\}$ upon which the solution $u_i\left(x_0, t_0\right)$ has a dependency. The CFL condition ensures that the domain of dependence of the exact solution to the partial differential equation is contained within the domain of dependence of the numerical solution. If the CFL condition is not satisfied, then the exact solution depends on a larger set of points than the numerical solution. In such case, changing the state in certain points may change the exact solution but not the numerical solution, and therefore the numerical solution cannot converge to the exact one.

4. Validation of the method using benchmark problems

In the numerical simulations to follow, we use sets of values from Table 1 as the moduli of the phases. These values were taken as representative values within the characteristic range of the values that fits elastomers, see, *e.g.*,Refs. [60–62], and the references therein. In the numerical examples to follow, we set the Courant number to 0.9.

We first test our scheme in Section 4.1 against the analytical solution for the problem of a finite layer that is released from an initial shear strain, while bounded between two semi-infinite layers with different parameters. In Section 4.2 we test it in a nonlinear problem of the scattering of an incident finite-amplitude shock wave from one half-space, impinging on an interface with a second half-space made of a different material.

4.1. Small-amplitude waves

Our first test case corresponds to a "fiber" of thickness $l = 0.1$ m with the property set 2 in Tab. 1, bounded by two semi-infinite "matrix"

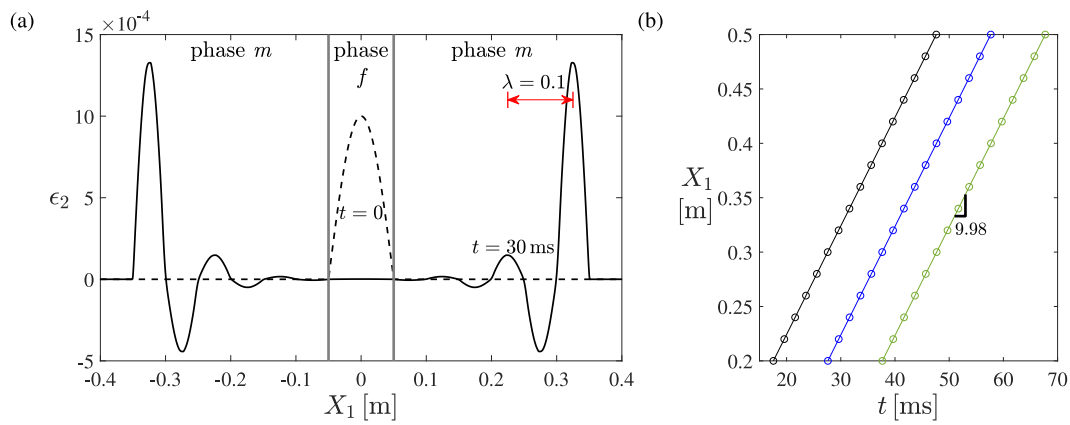

Fig. 3. (a) The distribution of ϵ_2 as function of X_1 at $t = 0$ (dash) and $t = 30$ ms (solid). (b) The location of each strain local peak in the domain $X_1 > 0.05$ as function of time.

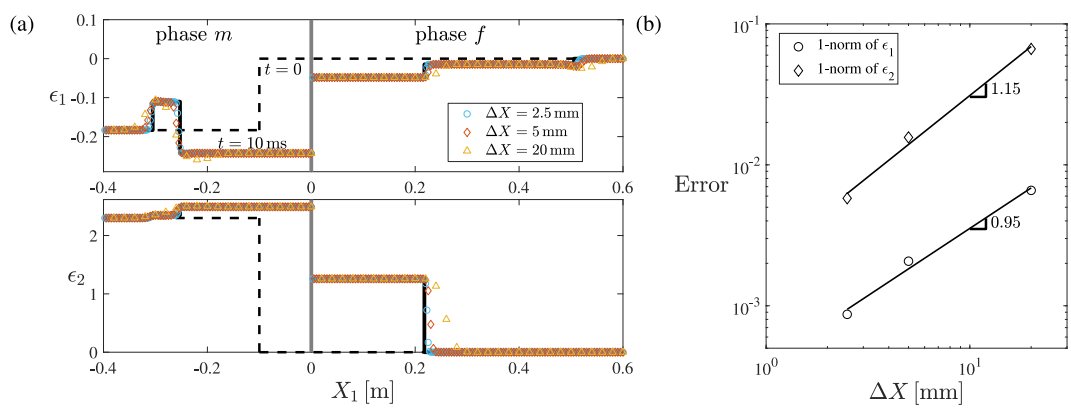

Fig. 4. (a) The strains of ϵ_1 and ϵ_2 at $t = 10$ ms for the shock scattering problem. The dashed line is the initial strain. The black line is the solution using Newton's method, and markers correspond to our finite-volume solutions with different grids. (b) The 1-norm of the errors of ϵ_1 (circles) and ϵ_2 (diamonds) as function of the cell length ΔX.

phases with the property set 1 in Tab. 1. The fiber is subjected to the infinitesimal initial strain field

$$\epsilon_2\left(X_1, t=0\right) = \begin{cases} 10^{-3}\cos\frac{\pi}{l}X_1, & -\frac{l}{2} < X_1 < \frac{l}{2}, \\ 0, & \text{elsewhere.} \end{cases} \tag{30}$$

This test case is similar to the test case by Bale et al. [34], with the difference that we prescribe initial shear instead of compression, and use nonlinear phases. The solution is obtained using our finite volume method with a grid of 2000 cells per meter ($\Delta X = 0.5$ mm).

Fig. 3(a) shows the shear strain ϵ_2 as function of X_1 at $t = 0$ (dashed line) and $t = 30$ ms (solid line). As discussed by Bale et al. [34], the initial strain is symmetrically separated into rightward and leftward propagating waves that repeatedly reflect and refract at the interfaces, thereby generating a train of (in this case shear) waves in the semi-infinite media. Note that ϵ_1 remains zero everywhere as it should in this uncoupled linear limit. The resultant waves are compared with the analytical solution for their length and velocity, see, *e.g.*, the derivation by Shmuel and Moiseyev [44]. We first present in panel (b) the location of each strain local peak in the domain $X_1 > 0.05$ as function of time. We observe that the curves are linear with the constant slope 9.98 ms^{-1}, which implies a 0.2% error with respect to the analytical value in the limit of small strains, namely, $c^{(m)} = \sqrt{\mu^{(m)}/\rho_L^{(m)}} = 10\,\text{ms}^{-1}$.

Next, we compare the wavelengths in the numerical simulation to the analytical prediction. According to Eq. (46) of Shmuel and Moiseyev [44], the allowed wavelength is $\lambda = 2lc^{(m)}/c^{(f)}$, where $c^{(f)} = \sqrt{\mu^{(f)}/\rho_L^{(f)}}$, yielding $\lambda = 0.1$ m for our parameters. The wavelength[6] as measured by the peak-to-peak distance in our numerical simulation is exactly 0.1 m between every adjacent peaks. The distance between the first and second peaks is illustrated for example in Fig. 3(a).

4.2. Finite shock scattering at the interface between two half-spaces

We consider the case of reflection and transmission of an incident shock wave of finite amplitude at an interface between two elastic half-spaces. This nonlinear benchmark problem is chosen since we are able to obtain for it numerical solutions using standard root-finding algorithms—and specifically Newton's method – which will be compared with our finite-volume method. We use sets 1 and 2 for the moduli of phase m (left half-space) and phase f (right half-space), respectively. The left half-space is subjected to a shock wave for which the pre-shock state is unstrained and at rest, and its post-shock state is $\left(\epsilon_1, \epsilon_2, v_1, v_2\right) \approx (-0.2, 2.3, 2.6, -32.4)$. These initial conditions were chosen to generate four shock waves, for which we obtain numerical solutions using Newton's method, as described by Ziv and Shmuel [7] and in the Appendix. Fig. 4(a) shows the distribution of ϵ_1 (upper panel) and ϵ_2 (lower panel) across $-0.4\,\text{m} < X_1 < 0.6\,\text{m}$ at $t = 10$ ms. The black line corresponds to the numerical solution of the exact equations. To

[6] Note that since the initial condition has a discontinuity in its derivative, it breaks down to rightward and leftward waves that also have discontinuous derivatives at their ends. The interference of their subsequent refractions and refractions yields strain fields in the m phases that also exhibit a discontinuous derivative.

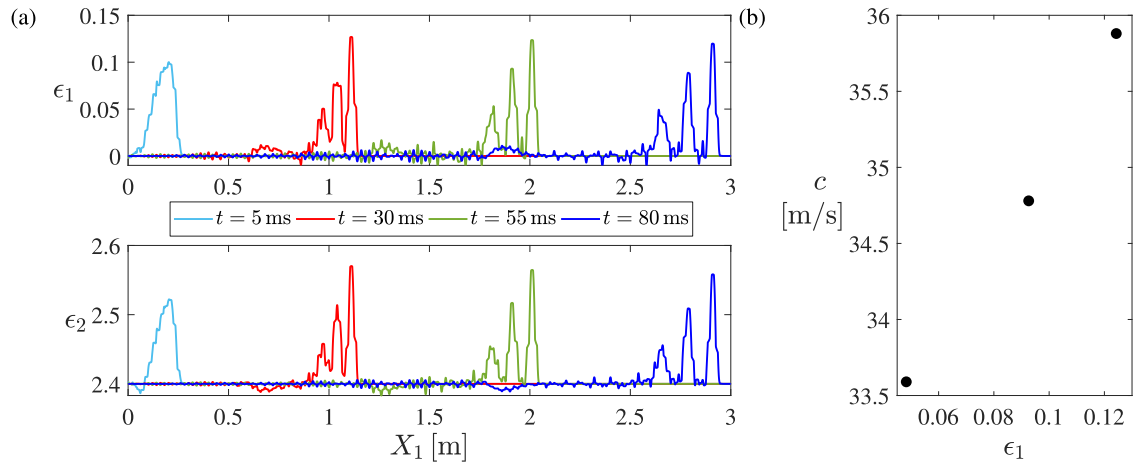

Fig. 5. (a) The strain distribution in the studied Gent laminate when subjected to axial-transverse strain. (b) The vector solitary wave velocity versus the maximal value of ϵ_1 at the middle of phase m over the time that the wave traverses a unit cell. (For interpretation of the references to color in this figure legend, the reader is referred to the web version of this article.)

test the convergence of our scheme, we compare solutions using three different grids, namely, $\Delta X = 20$ (orange triangles), 5 (red diamonds) and 2.5 mm (blue circles). It is clear that upon refining the grid, our scheme converges to the "exact" solution, which is partially covered by the marks in the figure. In order to quantify the rate of convergence, we calculate the 1-norm of the error E between the two solutions, defined by

$$\|E\|_1 = \Delta X \sum_i \left|\mathsf{q}^{(i)} - \mathsf{q}\left(X_1 = i\Delta X\right)\right|, \tag{31}$$

where q is the "exact" solution. Fig. 4(b) shows the 1-norm of the errors of ϵ_1 (circles) and ϵ_2 (diamonds) as function of the cell length ΔX for each one of the three grids depicted in Fig. 4(a). The slope of the norms are around 1 in a logarithmic scale, indicating that the rate of convergence of the numerical solution is approximately of first order. This is expected since the second order correction of the method is neglected in the vicinity of discontinuities, where this solution consists of discontinuities only.

A feature worth noting is the propagation of ϵ_1 without ϵ_2, as shown at $X_1 = 0.5$. This propagation is associated with the quasi-pressure wave, which does not exhibit axial-transverse strain coupling in the absence of pre-shear. As detailed by Ziv and Shmuel [7] in Sec. 2.1 therein, this coupling is given by

$$\frac{\partial \epsilon_2}{\partial \epsilon_1} = \frac{\epsilon_+^2 - \alpha}{\beta}, \tag{32}$$

together with the compatibility (initial) condition. In our case, phase f is not pre-sheared and we have that

$$\lim_{\epsilon_2(t=0)\to 0} \frac{\partial \epsilon_2}{\partial \epsilon_1} = 0, \tag{33}$$

i.e., the strains are not coupled. Phase m is pre-sheared, so the discontinuities in ϵ_1 and ϵ_2 occur simultaneously with respect to X_1. Fig. 6b of Ziv and Shmuel [7] exhibits the same feature, where shocks in homogeneous soft media were studied. By contrast, a similar analysis for the quasi-shear waves shows that the strain components are coupled even in the absence of pre-shear. Hence, the two strains are coupled during the propagation of the quasi-shear wave. Since this wave is slower than the pressure waves, this simultaneous spatial discontinuity in ϵ_1 and ϵ_2 occurs at X_1 which is smaller than $X_1 = 0.5$.

5. Numerical experiments of coupled waves in nonlinear laminates

We consider an infinite laminate composed of two alternating m and f compressible Gent layers with an equal length of $H^{(m)} = H^{(f)} = 1$ cm. We use sets 3 and 4 in Table 1 for the moduli of phases m and f, respectively. Note that these sets differ only in the mass density; as we show in the sequel, the modulation of this single property is sufficient for the medium to support vector solitary waves. The laminate is subjected to the initial strain field

$$\epsilon_i\left(X_1, t=0\right) = \begin{cases} \epsilon_i^{(I)} + A_i \cos\frac{\pi}{w} X_1, & -\frac{w}{2} < X_1 < \frac{w}{2}, \\ \epsilon_i^{(I)}, & \text{elsewhere}, \end{cases} \tag{34}$$

where $\epsilon_i^{(I)}$, A_i and w are prescribed quantities, and the values of i depend on the type of displacements considered, as described next.

Coupled axial and transverse displacements.—Here, i takes the values 1 and 2, and we set

$$\epsilon_1^{(I)} = 0,\ \epsilon_2^{(I)} = 2.4,\ A_1 = A_2 = 0.2, w = 0.19\,\text{m}. \tag{35}$$

Fig. 5 shows ϵ_1 and ϵ_2 as functions of X_1, using a grid of 2000 cells per meter ($\Delta X = 0.5$ mm), such that each layer is discretized to 20 cells. Cyan, red, green and blue lines correspond to $t = 5$, 30, 55 and 80 ms, respectively. Remarkably, the rightward propagating wave[7] is separated into a train of vector solitary waves, maintaining both their profile of the axial and shear components at the different periodic cells. This observation of *vector* solitary waves in Gent laminates follows the observation of scalar pressure solitary waves in nonlinear laminates by LeVeque [33] and LeVeque and Yong [38]. Interestingly, we observe that the width of each vector solitary waves is approximately ten layers, similarly to the width reported by LeVeque and Yong [38] in the scalar case. While not shown here, we note that the number of generated solitary waves increases for greater values of w, as is the case for the KdV solitary waves.

The dependency of the vector solitary wave velocity on the strain amplitude is studied in panel (b). Specifically, we show the velocity against the maximal value of ϵ_1 in the middle of phase m over the time that the solitary wave traverses a unit cell. We observe that the velocity is a monotonically increasing function of the strain amplitude. This dependency is in opposite of the dependency of the vector solitary waves discovered by Deng et al. [52] in the discrete mechanical system they conceived, and similar to the dependency of the KdV solitons and the dependency observed by LeVeque and Yong [38].

Coupled transverse displacements in two dimensions.—In this case $i = 2$ and 3, and we set

$$\epsilon_2^{(I)} = 1,\ \epsilon_3^{(I)} = 0,\ A_2 = 0,\ A_3 = 2,\ w = 0.2\,\text{m}. \tag{36}$$

[7] Owing to the symmetry of the problem, a mirrored wave that is propagating to the left is also generated.

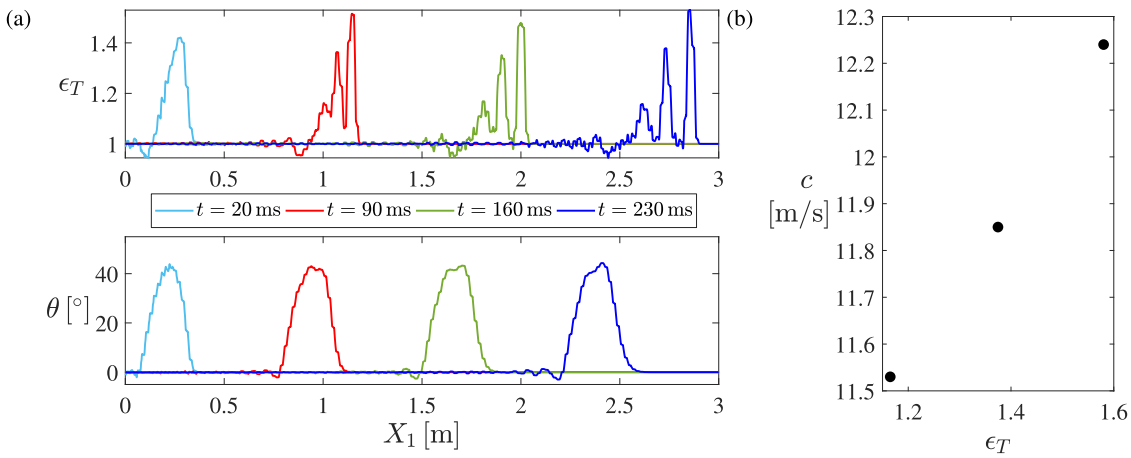

Fig. 6. (a) The distribution of ϵ_T and θ in the studied laminate when subjected to transverse–transverse strain. (b) The linearly polarized solitary wave velocity versus the maximal value of ϵ_T at the middle of phase m over the time that the wave traverses a unit cell. (For interpretation of the references to color in this figure legend, the reader is referred to the web version of this article.)

Fig. 6 shows ϵ_T and θ as functions of X_1, using a grid of 2000 cells per meter. Cyan, red, green and blue lines correspond to $t = 20$, 90, 160 and 230 ms, respectively. We observe that the transformation (18) proves useful also here, as it exposes two uncoupled polarizations of different nature. Specifically, its shows a linear polarization associated with ϵ_T that breaks up into a train of three solitary waves with similar shape and different magnitude and velocity. The distance between each peak and its following peak is increasing in time, implying that the velocity is higher at higher strains. This is quantified in panel (b), where the velocity of the linearly polarized solitary waves is plotted against the maximal value of ϵ_T at the middle of phase m over the time that the solitary wave traverses a unit cell. The second polarization associated with θ which lags behind the solitary waves is circular, and propagates effectively as a linear wave as it does *not* break up into θ-dependent waves; while not shown here for brevity, this occurs independently of the width of the initial localized strain w. Since the circular polarization is of linear waves, and it propagates independently of the linearly polarized solitary waves, the latter are scalar solitary waves and not vector solitary waves, even though they propagate through two coupled components of the displacement vector field.

6. Summary

We have developed a designated scheme to numerically solve the equations that govern elastic waves with two coupled components of finite amplitude in laminates made of nonlinear layers. Our scheme is based on two main elements. The first one is loaned from LeVeque [29], whose finite-volume method utilizes the solution of a Riemann problem at the interface between grid cells to solve nonlinear hyperbolic systems that are not in conservation form. The second element is the flux-based wave decomposition of LeVeque [33] and Bale et al. [34]. Our extension required accounting for the generation of additional waves with respect to the acoustic problems of single stress component that were addressed by LeVeque [33] and Bale et al. [34]. This was carried out using a suitable matrix formulation which captures the coupling between the different components of the displacement and stress fields. We have specifically addressed two cases, namely, a motion with coupling between its axial and transverse components, and a motion with two coupled transverse components.

We first tested our method using two benchmark problems. The first problem is linear, as there the initial strain is infinitesimal, and indeed our scheme recovered the analytical solution for the velocity and length of the generated waves. The second test case is of nonlinear waves and therefore more challenging. Specifically, we considered an incident shock of finite amplitude that strikes an interface between two half-spaces made of different nonlinear materials. The constitutive response of the half-spaces is described by the compressible Gent model [46,56]; in our previous work [7] we have demonstrated that this model is capable of capturing shear shock waves and tensile-induced shocks phenomena in soft materials, which were observed experimentally by Catheline et al. [47], Espíndola et al. [48], and Niemczura and Ravi-Chandar [49], respectively. For this problem, numerical solutions using standard root-finding algorithms are accessible, and a comparison between such solutions using Newton's method and our method has shown an excellent agreement between the two solutions. This was the first numerical experiment of shock scattering between two half-spaces in finite elastodynamics with two coupled components.

Subsequently, we have applied our scheme in a numerical experiment of finite-amplitude waves with two coupled components in an initially strained periodic laminate made of two alternating compressible Gent layers. In the case of coupled axial and transverse displacements, our experiment revealed the generation of vector solitary waves. To the best of our knowledge, this is the first observation of vector solitary waves within the framework of *continuum* solid mechanics. Our observation was preceded by the first construction of vector solitary waves in *discrete* mechanical systems by Deng et al. [13,52,53]. There, the model is a periodic repetition of rigid squares that are interlinked by springs, thereby supporting transitional and rotational waves. Interestingly, while these vectorial mechanical waves are slower at higher amplitudes, the vector waves in our continuum laminated model are faster at higher amplitudes. Therefore, the vector solitary waves here are more similar to KdV solitons and the acoustic solitary waves analyzed by LeVeque and Yong [38].

In the case of a coupling between two displacement components in the plane of the layers, our numerical experiment revealed the generation of a linearly degenerate wave of circular polarization that lags behind a train of solitary waves with linear polarization. Here again, the solitary waves are faster at higher amplitudes.

We believe that this paper establishes a starting point for several future works, among which we list the development of related higher-other methods such as the weighted essentially non-oscillatory (WENO) finite difference, see the survey by Shu [63] and the references therein; methods and studies concerning higher-dimensional problems [29,34,43,64]; analytical investigations using homogenization approaches [38,64,65]; and the introduction of a kinematic split between the isochoric

and volumetric parts of the motion into the method, which is useful when the volumetric stiffness is several orders of magnitude greater than the shear stiffness [66,67].

Declaration of competing interest

The authors declare that they have no known competing financial interests or personal relationships that could have appeared to influence the work reported in this paper.

Acknowledgments

We are very grateful to anonymous reviewers who significantly helped improving this paper through many constructive comments on its first version. We also acknowledge the support of the Israel Science Foundation, funded by the Israel Academy of Sciences and Humanities (Grant no. 1912/15), the United States-Israel Binational Science Foundation, Israel (Grant no. 2014358), and Ministry of Science and Technology, Israel (grant no. 880011).

Appendix. Solution to a transmission problem between two half-spaces

The general solution to the interface problem formulated in Section 4.2 consists of four waves, namely, two leftward propagating waves and two rightward propagating waves. For smooth waves to propagate, the velocity at the tail of the wave should be smaller than the velocity at the wavefront, and its change in-between should be monotonic. As described by Ziv and Shmuel [7] and the references therein, shock waves form when these conditions fail; see also the work of Berjamin et al. [68] for the one-dimensional case. Specifically for this problem which involves quasi-shear and pressure waves, in each medium there are four different combinations of ways these waves may evolve, namely, smooth–smooth, shock–smooth, smooth–shock, and shock–shock. To determine which combination takes place, one approach is to use a semi-inverse method, namely, assume a solution, examine the compatibility of the relevant equations, and proceed to the next possible combination if the equations are not compatible (see the paper by Ziv and Shmuel [7], for more details). For the shock–shock combination, the corresponding jump conditions across each shock are [14]

$$\begin{aligned} &\rho_L[\![v_1]\!]V + [\![P_{11}]\!] = 0,\ [\![\epsilon_1]\!]V + [\![v_1]\!] = 0,\\ &\rho_L[\![v_2]\!]V + [\![P_{21}]\!] = 0,\ [\![\epsilon_2]\!]V + [\![v_2]\!] = 0, \end{aligned} \tag{A.1}$$

where $[\![\circ]\!]$ is the jump in $(\circ)$ ahead and behind the shock and V is the shock velocity. The continuity of the velocity and traction at the interface is

$$\begin{pmatrix} v_1^{(m)} \\ v_2^{(m)} \\ P_{11}^{(m)} \\ P_{21}^{(m)} \end{pmatrix} = \begin{pmatrix} v_1^{(f)} \\ v_2^{(f)} \\ P_{11}^{(f)} \\ P_{21}^{(f)} \end{pmatrix}. \tag{A.2}$$

In order for this solution of the four shock waves to be stable, *i.e.*, when the waves will remain to propagate as shocks, certain entropy conditions must be satisfied. These conditions require that the wave velocity is greater behind the shock than ahead of the shock, namely,

$$c_\pm\left(\epsilon_1 = \epsilon_1^{(\text{ahead})},\ \epsilon_2 = \epsilon_2^{(\text{ahead})}\right) < V < c_\pm\left(\epsilon_1 = \epsilon_1^{(\text{behind})},\ \epsilon_2 = \epsilon_2^{(\text{behind})}\right), \tag{A.3}$$

Eqs. (A.1) and (A.2) yield 20 equations for determining 16 field variables and 4 shock velocities. The components v_1, v_2, P_{11}, and P_{21} are nonlinear functions of the deformation, hence closed-form solutions are not accessible. The numerical solution to the interface problem formulated in Section 4.2 is obtained with Newton's method using the commercial software Mathematica 11.3 [69].

References

[1] Amit Bandyopadhyay, Sahar Vahabzadeh, Anish Shivaram, Susmita Bose, Three-dimensional printing of biomaterials and soft materials, MRS Bull. (ISSN: 0883-7694) 40 (12) (2015) 1162–1169, http://dx.doi.org/10.1557/mrs.2015.274.

[2] R.L. Truby, J.A. Lewis, Printing soft matter in three dimensions, Nature 540 (2016) 371–378.

[3] Katia Bertoldi, Vincenzo Vitelli, Johan Christensen, Martin van Hecke, Flexible mechanical metamaterials, Nat. Rev. Mater. 2 (11) (2017) 17066.

[4] N. Nadkarni, C. Daraio, D.M. Kochmann, Dynamics of periodic mechanical structures containing bistable elastic elements: From elastic to solitary wave propagation, Phys. Rev. E 90 (2) (2014) 23204, http://dx.doi.org/10.1103/PhysRevE.90.023204, URL http://link.aps.org/doi/10.1103/PhysRevE.90.023204.

[5] Neel Nadkarni, Andres F. Arrieta, Christopher Chong, Dennis M. Kochmann, Chiara Daraio, Unidirectional transition waves in bistable lattices, Phys. Rev. Lett. 116 (24) (2016) 244501.

[6] Alexander M. Samsonov, Irina V. Semenova, Fedor E. Garbuzov, Nonlinear guided bulk waves in heterogeneous elastic structural elements, Int. J. Non-Linear Mech. 94 (2017) 343–350.

[7] Ron Ziv, Gal Shmuel, Smooth waves and shocks of finite amplitude in soft materials, Mech. Mater. (ISSN: 0167-6636) 135 (2019) 67–76, http://dx.doi.org/10.1016/j.mechmat.2019.05.002, URL http://www.sciencedirect.com/science/article/pii/S016766361930002X.

[8] Bolei Deng, Chengyang Mo, Vincent Tournat, Katia Bertoldi, Jordan R. Raney, Focusing and mode separation of elastic vector solitons in a 2d soft mechanical metamaterial, Phys. Rev. Lett. 123 (2) (2019) 024101a.

[9] Shmuel Katz, Sefi Givli, Solitary waves in a nonintegrable chain with double-well potentials, Phys. Rev. E 100 (2019) 032209, http://dx.doi.org/10.1103/PhysRevE.100.032209, URL https://link.aps.org/doi/10.1103/PhysRevE.100.032209.

[10] J. Raney, N. Nadkarni, C. Daraio, D.M. Kochmann, J.A. Lewis, K. Bertoldi, Stable propagation of mechanical signals in soft media using stored elastic energy, Proc. Natl. Acad. Sci. USA. (2016).

[11] Hiromi Yasuda, Yasuhiro Miyazawa, Efstathios G. Charalampidis, Christopher Chong, Panayotis G. Kevrekidis, Jinkyu Yang, Origami-based impact mitigation via rarefaction solitary wave creation, Sci. Adv. 5 (5) (2019) eaau2835.

[12] Myungwon Hwang, Andres F. Arrieta, Input-independent energy harvesting in bistable lattices from transition waves, Sci. Rep. 8 (1) (2018) 3630.

[13] Bolei Deng, Pai Wang, Qi He, Vincent Tournat, Katia Bertoldi, Metamaterials with amplitude gaps for elastic solitons, Nat. Commun. 9 (1) (2018) 3410.

[14] L. Davison, Propagation of plane waves of finite amplitude in elastic solids, J. Mech. Phys. Solids (ISSN: 0022-5096) 14 (5) (1966) 249–270, http://dx.doi.org/10.1016/0022-5096(66)90022-6, URL http://www.sciencedirect.com/science/article/pii/0022509666900226.

[15] Michael M. Carroll, Some results on finite amplitude elastic waves, Acta Mech. 3 (2) (1967) 167–181.

[16] Michel Destrade, Giuseppe Saccomandi, Finite amplitude elastic waves propagating in compressible solids, Phys. Rev. E 72 (1) (2005) 16620.

[17] S. Chockalingam, T. Cohen, Shear shock evolution in incompressible soft solids, J. Mech. Phys. Solids (ISSN: 0022-5096) 134 (2020) 103746, http://dx.doi.org/10.1016/j.jmps.2019.103746, URL http://www.sciencedirect.com/science/article/pii/S0022509619306684.

[18] Douglas S. Drumheller, Introduction to Wave Propagation in Nonlinear Fluids and Solids, Cambridge University Press, Cambridge, ISBN: 9780521587464, 1998, http://dx.doi.org/10.1017/CBO9781139174893, URL https://www.cambridge.org/core/books/introduction-to-wave-propagation-in-nonlinear-fluids-and-solids/4E630F47CFC8D05C86766C5E46C4410C.

[19] Gilles Kluth, Bruno Després, 2d finite volume lagrangian scheme in hyperelasticity and finite plasticity, in: unilla Kreiss, Per Lötstedt, Axel Målqvist, Maya Neytcheva (Eds.), Numerical Mathematics and Advanced Applications 2009, Springer Berlin Heidelberg, Berlin, Heidelberg, ISBN: 978-3-642-11795-4, 2010, pp. 489–496.

[20] Javier Bonet, Antonio J. Gil, Rogelio Ortigosa, A computational framework for polyconvex large strain elasticity, Comput. Methods Appl. Mech. Engrg. 283 (2015) 1061–1094, http://dx.doi.org/10.1016/j.cma.2014.10.002, URL http://www.sciencedirect.com/science/article/pii/S0045782514003636.

[21] Jacob Aboudi, Yako Benveniste, One-dimensional finite amplitude wave propagation in a compressible elastic half-space, Int. J. Solids Struct. (ISSN: 0020-7683) 9 (3) (1973) 363–378, http://dx.doi.org/10.1016/0020-7683(73)90086-3, URL http://www.sciencedirect.com/science/article/pii/0020768373900863.

[22] Olivier Bou Matar, Pierre-Yves Guerder, YiFeng Li, Bart Vandewoestyne, Koen Van Den Abeele, A nodal discontinuous galerkin finite element method for nonlinear elastic wave propagation, J. Acoust. Soc. Am. 131 (5) (2012) 3650–3663, http://dx.doi.org/10.1121/1.3693654.

[23] Harold Berjamin, Bruno Lombard, Guillaume Chiavassa, Nicolas Favrie, A finite-volume approach to 1d nonlinear elastic waves: Application to slow dynamics, Acta Acust. United Acust. 104 (4) (2018) 561–570.

[24] E. Godlewski, P.A. Raviart, Numerical Approximation of Hyperbolic Systems of Conservation Laws, in: Number 118 in Applied Mathematical Sciences, Springer, ISBN: 9780387945293, 1996, URL https://books.google.co.il/books?id=9BwMIDMmTmcC.

[25] Eleuterio F. Toro, Riemann Solvers and Numerical Methods for Fluid Dynamics, 1997.

[26] J.A. Trangenstein, Numerical Solution of Hyperbolic Partial Differential Equations, Cambridge University Press, ISBN: 9780521877275, 2009.

[27] Randall J. LeVeque, Finite Volume Methods for Hyperbolic Problems, Cambridge University Press, Cambridge, ISBN: 9780521009249, 2002, http://dx.doi.org/10.1017/CBO9780511791253, URL https://www.cambridge.org/core/books/finite-volume-methods-for-hyperbolic-problems/97D5D1ACB1926DA1D4D52EAD6909E2B9.

[28] Peter Lax, Burton Wendroff, Systems of conservation laws, Commun. Pure Appl. Math. 13 (2) (1960) 217–237.

[29] Randall J. LeVeque, Wave propagation algorithms for multidimensional hyperbolic systems, J. Comput. Phys. (ISSN: 0021-9991) 131 (2) (1997) 327–353, http://dx.doi.org/10.1006/jcph.1996.5603.

[30] Arkadi Berezovski, GA Maugin, Simulation of thermoelastic wave propagation by means of a composite wave-propagation algorithm, J. Comput. Phys. 168 (1) (2001) 249–264.

[31] Philip Trevor Barton, Dimitris Drikakis, E.I. Romenski, An Eulerian finite-volume scheme for large elastoplastic deformations in solids, Internat. J. Numer. Methods Engrg. 81 (4) (2010) 453–484.

[32] Tiernan R. Fogarty, Randall J. LeVeque, High-resolution finite-volume methods for acoustic waves in periodic and random media, J. Acoust. Soc. Am. 106 (1) (1999) 17–28.

[33] Randall J. LeVeque, Finite-volume methods for non-linear elasticity in heterogeneous media, Int. J. Numer. Methods Fluids 40 (1–2) (2002) 93–104.

[34] D.S. Bale, R.J. Leveque, S. Mitran, J.A. Rossmanith, A wave propagation method for conservation laws and balance laws with spatially varying flux functions, SIAM J. Sci. Comput. (ISSN: 1064-8275) 24 (3) (2002) 955–978, http://dx.doi.org/10.1137/S106482750139738X.

[35] Thierry Dauxois, Michel Peyrard, Physics of Solitons, Cambridge University Press, 2006.

[36] M.I. Hussein, R. Khajehtourian, Nonlinear bloch waves and balance between hardening and softening dispersion, Proc. R. Soc. Lond. Ser. A Math. Phys. Eng. Sci. 474 (2217) (2018) 20180173.

[37] Randall J. LeVeque, Darryl H. Yong, Phase plane behavior of solitary waves in nonlinear layered media, in: Hyperbolic Problems: Theory, Numerics, Applications, Springer, 2003, pp. 43–51.

[38] Randall J. LeVeque, Darryl H. Yong, Solitary waves in layered nonlinear media, SIAM J. Appl. Math. 63 (5) (2003) 1539–1560.

[39] J. Engelbrecht, A. Berezovski, A. Salupere, Nonlinear deformation waves in solids and dispersion, Wave Motion (ISSN: 0165-2125) 44 (6) (2007) 493–500, http://dx.doi.org/10.1016/j.wavemoti.2007.02.006, Special Issue of Selected Papers Presented at the International Symposium on Mechanical Waves in Solids, URL http://www.sciencedirect.com/science/article/pii/S0165212507000224.

[40] Zhenli Xu, Peng Zhang, Ruxun Liu, δ-Mapping algorithm coupled with weno reconstruction for nonlinear elasticity in heterogeneous media, Appl. Numer. Math. (ISSN: 0168-9274) 57 (1) (2007) 103–116, http://dx.doi.org/10.1016/j.apnum.2006.01.003, URL http://www.sciencedirect.com/science/article/pii/S0168927406000055.

[41] Ben Lustig, Guy Elbaz, Alan Muhafra, Gal Shmuel, Anomalous energy transport in laminates with exceptional points, J. Mech. Phys. Solids (ISSN: 0022-5096) (2019) 103719, http://dx.doi.org/10.1016/j.jmps.2019.103719, URL http://www.sciencedirect.com/science/article/pii/S0022509619306921.

[42] W.D. Collins, One-dimensional non-linear wave propagation in incompressible elastic materials, Quart. J. Mech. Appl. Math. 19 (3) (1966) 259–328.

[43] Harold Berjamin, Bruno Lombard, Guillaume Chiavassa, Nicolas Favrie, Plane-strain waves in nonlinear elastic solids with softening, Wave Motion 89 (2019) 65–78.

[44] Gal Shmuel, Nimrod Moiseyev, Linking scalar elastodynamics and non-hermitian quantum mechanics, Phys. Rev. Appl. 13 (2020) 024074, http://dx.doi.org/10.1103/PhysRevApplied.13.024074, URL https://link.aps.org/doi/10.1103/PhysRevApplied.13.024074.

[45] Lee Davison, Fundamentals of Shock Wave Propagation in Solids, Springer-Verlag Berlin Heidelberg, 2008.

[46] A.N. Gent, A new constitutive relation for rubber, Rubber Chem. Technol. 69 (1996) 59–61.

[47] S. Catheline, J.-L. Gennisson, M. Tanter, M. Fink, Observation of shock transverse waves in elastic media, Phys. Rev. Lett. 91 (2003) 164301, http://dx.doi.org/10.1103/PhysRevLett.91.164301, https://link.aps.org/doi/10.1103/PhysRevLett.91.164301.

[48] David Espíndola, Stephen Lee, Gianmarco Pinton, Shear shock waves observed in the brain, Phys. Rev. A 8 (4) (2017) 044024.

[49] J. Niemczura, K. Ravi-Chandar, On the response of rubbers at high strain rates—II. Shock waves, J. Mech. Phys. Solids (ISSN: 0022-5096) 59 (2) (2011) 442–456, http://dx.doi.org/10.1016/j.jmps.2010.09.007, URL http://www.sciencedirect.com/science/article/pii/S0022509610001833.

[50] Yijiang Chen, Stability of vector solitary waves, Phys. Rev. A 50 (1994) 5205–5208, http://dx.doi.org/10.1103/PhysRevA.50.5205, URL https://link.aps.org/doi/10.1103/PhysRevA.50.5205.

[51] Zhigang Chen, Mordechai Segev, Demetrios N. Christodoulides, Optical spatial solitons: historical overview and recent advances, 75 (8), 2012, p. 086401, http://dx.doi.org/10.1088/0034-4885/75/8/086401.

[52] B. Deng, J.R. Raney, V. Tournat, K. Bertoldi, Elastic vector solitons in soft architected materials, Phys. Rev. Lett. 118 (2017) 204102.

[53] Bolei Deng, Vincent Tournat, Pai Wang, Katia Bertoldi, Anomalous collisions of elastic vector solitons in mechanical metamaterials, Phys. Rev. Lett. 122 (2019) 044101b.

[54] R.W. Ogden, Non-Linear Elastic Deformations, Dover Publications, New York, 1997.

[55] J. Bonet, R.D. Wood, Nonlinear Continuum Mechanics for Finite Elements Analysis, Cambridge University Press, 1997.

[56] O. Lopez-Pamies, P. Ponte Castañeda, Homogenization-based constitutive models for porous elastomers and implications for macroscopic instabilities: Ii—results, J. Mech. Phys. Solids (ISSN: 0022-5096) 55 (8) (2007) 1702–1728, http://dx.doi.org/10.1016/j.jmps.2007.01.008, URL http://www.sciencedirect.com/science/article/pii/S0022509607000269.

[57] Cornelius O. Horgan, The remarkable Gent constitutive model for hyperelastic materials, Int. J. Non-Linear Mech. (ISSN: 0020-7462) 68 (2015) 9–16, http://dx.doi.org/10.1016/j.ijnonlinmec.2014.05.010, URL http://www.sciencedirect.com/science/article/pii/S0020746214001127.

[58] Sergei Konstantinovich Godunov, A difference method for numerical calculation of discontinuous solutions of the equations of hydrodynamics, Mat. Sb. 89 (3) (1959) 271–306.

[59] Richard Courant, Kurt Friedrichs, Hans Lewy, On the partial difference equations of mathematical physics, IBM J. Res. Dev. 11 (2) (1967) 215–234.

[60] G. Marckmann, E. Verron, Comparison of hyperelastic models for rubber-like materials, Rubber Chem. Technol. 79 (5) (2006) 835–858, http://dx.doi.org/10.5254/1.3547969, 2020/02/16.

[61] F. Carpi, D. De Rossi, R. Kornbluh, R. Pelrine, P. Sommer-Larsen, Dielectric Elastomers As Electromechanical Transducers: Fundamentals, Materials, Devices, Models and Applications of an Emerging Electroactive Polymer Technology, Elsevier Science, ISBN: 978-0-08-047488-5, 2008.

[62] R. Getz, D.M. Kochmann, G. Shmuel, Voltage-controlled complete stopbands in two-dimensional soft dielectrics, Int. J. Solids Struct. (ISSN: 0020-7683) 113–114 (2017) 24–36, http://dx.doi.org/10.1016/j.ijsolstr.2016.10.002, URL http://www.sciencedirect.com/science/article/pii/S0020768316302931.

[63] Chi-Wang Shu, High order weno and dg methods for time-dependent convection-dominated pdes: A brief survey of several recent developments, J. Comput. Phys. 316 (2016) 598–613, http://dx.doi.org/10.1016/j.jcp.2016.04.030, URL http://www.sciencedirect.com/science/article/pii/S0021999116300766.

[64] Manuel Quezada de Luna, David I. DavKetcheson, Two-dimensional wave propagation in layered periodic media, SIAM J. Appl. Math. 74 (6) (2014) 1852–1869, http://dx.doi.org/10.1137/130937962, 2020/02/17.

[65] Igor V. Andrianov, Vladyslav V. Danishevs' kyy, Heiko Topol, Dieter Weichert, Homogenization of a 1d nonlinear dynamical problem for periodic composites, ZAMM-J. Appl. Math. Mech. 91 (6) (2011) 523–534.

[66] G.A. Holzapfel, Nonlinear Solid Mechanics: A Continuum Approach for Engineering, Wiley, ISBN: 9780471823193, 2000, URL https://books.google.co.il/books?id=_ZkeAQAAIAAJ.

[67] Fran,cois Peyraut, Zhi-Qiang Feng, Nadia Labed, A material-independent algorithm for preserving of the orientation of the spatial basis attached to deforming medium, Comput. Mech. 40 (6) (2007) 1053–1060, http://dx.doi.org/10.1007/s00466-007-0163-0.

[68] Harold Berjamin, Bruno Lombard, Guillaume Chiavassa, Nicolas Favrie, Analytical solution to 1d nonlinear elastodynamics with general constitutive laws, Wave Motion 74 (2017) 35–55, http://dx.doi.org/10.1016/j.wavemoti.2017.06.006, URL http://www.sciencedirect.com/science/article/pii/S016521251730077X.

[69] Wolfram Research, Inc., Mathematica 11.3, URL https://www.wolfram.com.